Self-generated cooperative light emission induced by atomic recoil

J. Javaloyes,[1,*] M. Perrin,[1,†] G. L. Lippi,[1] and A. Politi[1,2]
[1]*Institut Non Linéaire de Nice, UMR 6618 CNRS, Université de Nice–Sophia Antipolis, 1361 Route des Lucioles, F-06560 Valbonne, France*
[2]*Istituto Nazionale di Ottica Applicata, Largo E. Fermi 6, 50125 Firenze, Italy*
(Received 17 November 2003; published 13 August 2004)

The interaction of an atomic gas confined inside a cavity containing a strong electromagnetic field is numerically and theoretically investigated in a regime where recoil effects are not negligible. The spontaneous appearance of a density grating (atomic bunching) accompanied by the onset of a coherent, back-propagating electromagnetic wave is found to be ruled by a continuous phase transition. Numerical tests allow us to convincingly prove that the transition is steered by the appearence of a periodic atomic density modulation. Consideration of different experimental relaxation mechanisms induces us to analyze the problem in nearly analytic form, in the large detuning limit, using both a Vlasov approach and a Fokker-Planck description. The application of our predictions to recent experimental findings, reported by Kruse *et al.* [Phys. Rev. Lett., **91** 183601 (2003)], yields a semiquantitative agreement with the observations.

DOI: 10.1103/PhysRevA.70.023405 PACS number(s): 42.50.Vk, 05.45.Xt, 05.65.+b, 42.65.Sf

I. INTRODUCTION

Recoil in the interaction between atoms and electromagnetic fields is almost exclusively associated with the idea that momentum transfer is a way of slowing down atoms to extremely low temperatures [1]. However, nontrivial consequences on light propagation have been uncovered as well. For instance, the amplification of a small probe field in the presence of a strong counterpropagating field was theoretically predicted already in [2] and experimentally observed in [3–5]. Recoil-induced resonances (RIRs) are further single-atom effects that have been investigated both theoretically [6] and experimentally [7].

Atomic recoil, in addition to amplifying an injected probe field, has been conjectured to collectively give rise to coherent propagation through back reflection from a spontaneously generated density grating: this is the so-called collective atomic recoil laser (CARL) [8]. According to Ref. [9], the two approaches (RIR and CARL) provide an equivalent description of the gain experienced by a small nonzero probe field.

The very first observation of *self-generated* backward emission was made in a ring cavity experiment [10], where the very low "transverse temperature" might have been responsible for CARL amplification. More detailed experimental accounts have been reported in Refs. [11,12], although it was not possible to establish whether the generation of the backward field was due to the spontaneous formation of a density grating, or vice versa. In fact, although it was later ascertained that recoil plays a prominent role [13] in the underlying physics [11,12], an alternative interpretation based on the formation of a standard polarization grating could not be entirely ruled out [14]. Only recently has the first convincing evidence of CARL been given in a beautiful experiment performed on a sample of cold rubidium atoms [15].

On the theoretical side, too, no final conclusion could be drawn about the CARL features, because the first model allowed only an investigation of the transient regime. Stationary states could first be obtained by including collisions with an external buffer gas [16]. By simulating a low-temperature (a few millikelvins) sodium vapor in the detuning range previously considered in the (numerical) literature, a nonequilibrium phase transition leading to a stationary nonzero backward field (above a given threshold) was therein identified. However, such a collective phenomenon could not be linked to the onset of a density grating, but rather to the creation of a nontrivial polarization grating [16].

The overall scenario has been observed also in a more general model accounting for the input-field dynamics [17] and has been successively clarified in [18] with the help of the elimination of the atomic variables; indeed, this step rendered possible the derivation of an effective free-energy potential for the backward field amplitude, thereby clearly showing the existence of a phase transition.

In this paper we show numerically and theoretically that this latter model also accounts for the CARL and allows one to understand its onset in terms of a continuous phase transition characterized by two effective variables. The resulting estimate of the critical point is compatible with the experimental results reported in [15]. The results presented here provide substantial and systematic progress toward a proof of the existence, in stable form, of a collective interaction, which, predicted years ago [8], had so far proven to be elusive.

More precisely, we investigate a transition that gives rise spontaneously (i.e., without an external probe field) to a coherent electromagnetic field counterpropagating with respect to the injected one. We choose to consider the ring-cavity-based model introduced in [19,17] for two reasons. On the one hand, the available single-pass model [8] has intrinsic

*Present address: ONT, Université Libre de Bruxelles, Campus de la Plaine, C.P. 231, B-1050 Bruxelles, Belgium.
†Present address: IEMN, Avenue Poincaré, B.P. 69, 59652 Villeneuve d'Ascq, France.

shortcomings [20], which may be of little consequence in particular circumstances, but which renders it nonetheless less attractive. On the other hand, the most recent experimental results [15], which to our knowledge can be considered at the present time as the first and only available observation of a true CARL system, have been obtained in a ring cavity. Hence, the choice of a bidirectional ring cavity model imposes itself.

One of the most delicate issues connected with a meaningful description of a CARL concerns the thermalization of the atomic kinetic energy. The absence of stationary states in the original model [8] was indeed due to the lack of interaction with a thermal bath. Here, we show that widely differing microscopic mechanisms (such as collisions, finite transit time in the interaction volume, "optical friction," etc.) all give rise to the same macroscopic scenario: a continuous phase transition leading to a finite counterpropagating field, therefore showing that the microscopic details of the thermalization mechanism are irrelevant for the observed transition. This is a standard occurrence in both equilibrium and nonequilibrium statistical mechanics, where the same scenario is observed even when the microscopic interactions with the environment are modeled by quite an abstract scheme such as the Nosé-Hoover thermostat [21].

The paper is organized as follows. Section II introduces the model we used in the investigation and discusses, in Sec. II A, the main physical relaxation mechanisms that may take place in an experiment. The appropriate modeling tools for analyzing the two main mechanisms are introduced here. Section III is devoted to a systematic numerical analysis which allows us to highlight the origin of the forces that give rise to a transition of the CARL type—i.e., caused by the appearance of a spatial density grating—as opposed to the one recently predicted [16,18], which is based on an unusual polarization grating and which is possibly responsible for high-temperature experimental observations [11,12]. The numerical approach makes it possible to isolate the different source terms and identify in which range of temperature each of them is predominant.

Analytical descriptions present the advantage of offering a better understanding of the physics driving the system. Since the full problem is obviously analytically unmanageable, it is useful to study some limiting situations. This is done in Sec. IV, where we consider the case of large detuning between fields and atomic resonances, which corresponds to the conditions of the experiment [15]. A large detuning not only allows us to work with strongly simplified analytical expressions, but also prevents the appearance of multiphoton gain peaks, as predicted in [2]. Furthermore, in this limit any difference due to a possible multilevel structure would be completely washed out, so that our two-level schematization is as reasonable as more accurate models that take into account the hyperfine structure.

In this spirit, we describe the perturbations introduced by transit broadening (Sec. IV A) and show the appearance of a second-order transition, which can be described by expanding the spatial inhomogeneities in Fourier modes. The first and most relevant mode coincides with the *bunching parameter*, previously introduced to quantify the density grating [8]. Losses introduced by an optical molasses are studied in Sec. IV B with the help of a Fokker-Planck equation that can be analytically solved in the large dissipation limit. Predictions resulting from the preceding analyses are offered in Sec. V, together with a comparison with the recent experimental results [15]. Some conclusions and perspectives are presented in Sec. VI.

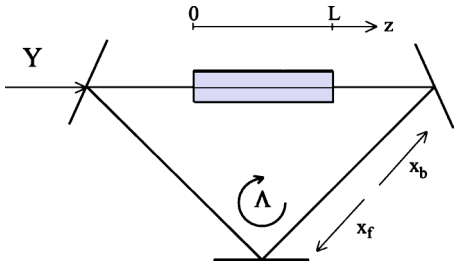

FIG. 1. Schematic representation of a bidirectional ring cavity. x_f and x_b denote the forward and backward fields, respectively, while Y is the amplitude of the injected field. The cell is filled by an optically active atomic vapor and a buffer gas (see Ref. [17] for further details).

II. MODEL

The starting model involves four dimensionless variables (one complex) accounting for the single-atom dynamics, plus two complex equations describing the amplitude of forward (x_f) and backward (x_b) uniform fields [17]

$$\begin{aligned}
\dot{\theta}_j &= p_j, \\
\dot{p}_j &= -\,\mathrm{Re}\{(x_f e^{i\theta_j} - x_b e^{-i\theta_j}) s_j^*\}(|\Delta_a|/2G), \\
\dot{s}_j &= G(x_f e^{i\theta_j} + x_b e^{-i\theta_j}) d_j - (\Gamma_\perp - i\Delta_a) s_j, \\
\dot{d}_j &= -\,G\ \mathrm{Re}\{(x_f e^{i\theta_j} + x_b e^{-i\theta_j}) s_j^*\} - \Gamma_\parallel (d_j + 1), \\
\dot{x}_f &= -\,(1 + i\Delta_c) x_f + Y + \tilde{C}\langle s e^{-i\theta}\rangle, \\
\dot{x}_b &= -\,(1 + i\Delta_c) x_b + \tilde{C}\langle s e^{i\theta}\rangle,
\end{aligned} \tag{1}$$

where $1 \leqslant j \leqslant N$ and the angular brackets denote an average over the atomic ensemble. Figure 1 shows a schematic representation of the geometry under consideration. Time and related parameters are expressed in units of the photon lifetime inside the cavity $(1/\kappa)$. The decay rates of the atomic polarization $(\Gamma_\perp)$ and population inversion $(\Gamma_\parallel)$, the detuning Δ_a between input field and atomic frequencies and the cavity detuning Δ_c (i.e., the distance from the nearest cavity resonance) are all dimensionless quantities. Moreover, $G = \sqrt{m\kappa|\Delta_a|/\hbar}/k$ and $\tilde{C} = \alpha\Gamma_\perp L/(G\mathcal{T})$ are the two coupling constants (m is the atomic mass, k the field wave number, α the unsaturated absorption rate per unit length, L the length of the atomic medium, and $\mathcal{T}$ the cavity's transmittivity). The amplitude Y of the injected field is scaled such that $Y^2 = 4\mathcal{D}^2\mathcal{P}/(AG^2\mathcal{T}\kappa^2\hbar^2)$, where $\mathcal{D}$ is the atomic dipole moment, $\mathcal{P}$ is the input power, and A is the beam surface, expressed in

physical units. An equivalent scaling is used for the forward and backward intracavity components x_f and x_b. Finally, (i) $\theta_j = kz_j$ is the scaled atomic position; (ii) The atomic momentum P_j is rescaled to $p_j = kP_j/(m\kappa)$; (iii) s_j and d_j are the atomic polarization and population inversion, the first being expressed in units of $\mathcal{D}$.

A. Relaxation mechanisms

While dissipation mechanisms affecting the internal degrees of freedom and the field amplitudes are accounted for by the above model, no losses acting on the atomic momentum are included therein. As a result, atoms are continuously accelerated by radiation pressure, and Eqs. (1) can thereby describe only the transient regime corresponding to the early stages of CARL amplification.

In actual experimental situations, relaxation processes may be induced by various mechanisms, the main ones being (a) collisions with a buffer gas (those between optically active atoms can be neglected under all realistic circumstances), (b) finite residence time in the interaction volume (added to some relaxation occurring outside it), and (c) "viscous" losses (e.g., as in an optical molasses). Collisions with a buffer gas require fairly high pressures and have often been used in the investigation of nonlinear coupling between atoms and light (cf., e.g., [22,23]). A precise modeling of collisions is a rather difficult task (cf., e.g., [35]). However, molecular dynamics simulations have long since taught that it is not necessary to accurately reproduce all microscopic details when the final goal is to provide a semi quantitative description of the macroscopic scenario [24]. In this specific case, extensive simulations performed with different schemes [25,26] indicate that only modest modifications in the position of the critical point have to be expected. Accordingly, we limit ourselves to defining below the simplest scheme we have adopted without pretending to provide a realistic description of each single collision.

A random sequence of intercollision times is independently generated for each atom according to an exponential distribution with average value equal to $1/\gamma_c$. At each collision, the momentum of the colliding, jth, atom is randomly reset according to the Gaussian distribution $Q_0(p_j) = \exp\{-p_j^2/(2T)\}/\sqrt{2\pi T}$ where $T = k_B \overline{T} k^2/(m\kappa^2)$ is the rescaled temperature of the buffer gas (k_B is Boltzmann's constant, $\overline{T}$ is the temperature in physical units); moreover, the phase of the atomic polarization s_j is also reset to a value uniformly distributed in the whole range $[0, 2\pi]$, as $|s_j|$ remains unchanged. Notice that this algorithm amounts to implicitly assuming that active and buffer-gas atoms have equal masses. This algorithm is the microscopic, molecular dynamics equivalent of the well known Bhatnagar-Gross-Krook truncation [36]. It amounts to replacing the collision term in the Boltzmann equation with a single term exponentially decaying toward local equilibrium. This approach has been proved to successfully model dilute gases [37].

The finite transit time (b) introduces effective losses and has certainly played the main role in several experiments [10–12]. In such a situation, the atoms spend a more or less small fraction of time inside the interaction volume, which they enter and exit at random positions and in a random state (both for the velocity and for the internal degrees of freedom). Outside the interaction region, the atoms suffer thermalization, either through collisions with other atoms (e.g., a low-pressure buffer gas) or with a container, or are simply renewed through "fresh" atoms coming from a beam; hence, the effective relaxation comes from the loss of "synchronized" atoms (both for the external and the internal degrees of freedom), compensated, on average, by the entrance into the interaction volume of "random" atoms. This phenomenon can be reinterpreted as a "reset" in the external and internal degrees of freedom of the atom in question. At the microscopic level, one can still adopt a description based on the thermalization scheme discussed in (a), by modeling each random exit and entrance in the active volume as a "collision;" the main difference from the previous case is that all atomic variables have now to be reset. At the macroscopic level, the mathematical tool most suited for such a description is a Vlasov equation, where the probability distributions for the atomic position and momentum are dynamically investigated. These considerations are the basis for the discussion of Sec. IV A.

The third mechanism (c), recently employed in [15], is an optical molasses, added in the experiment to obtain steady state backward emission. Here, the "molasses field" slows down the atoms by the standard cooling action while introducing a "friction" which prevents the Doppler shift from growing so large as to render the interaction with the field entirely negligible. It has been shown [27] that, under the assumption of a small saturation parameter of the molasses field, the momentum dynamics is well described by a Langevin equation [compare with the second of Eqs. (1)]

$$\dot{p}_j = \mathrm{Re}[(x_b e^{-i\theta_j} - x_f e^{i\theta_j}) s_j^*](|\Delta_a|/2G) - \gamma p_j + \eta_j, \qquad (2)$$

where η_j is a standard white noise

$$\langle \eta_j(t) \rangle = 0,$$

$$\langle \eta_j(t_1)\, \eta_k(t_2) \rangle = 2\gamma T \delta_{jk} \delta(t_1 - t_2) \qquad (3)$$

(δ_{jk} is the Kronecker symbol), accounting for the inevitable fluctuations that thermalize the atom to a finite temperature T. In Sec. IV B, we will study this model in the limit of large detuning, a condition well satisfied in the experiment [15].

III. NUMERICAL RESULTS

We now intend to explore the predictions of the model Eqs. (1) from a purely numerical point of view to provide a starting point for the later analysis. In particular, we are interested in studying the existence of a *steady state bunching* in the presence of a backward propagating field. We remark that the observation of a stable value of bunching in a bidirectional ring cavity has never been reported. Previous observations, obtained without a cavity [8], have shown a strongly oscillating, irregular behavior for this variable. In the other kind of observed transition [16,17], instead, the θ distribution remains flat (within the fluctuations imposed by the sample size) both below and above threshold. Hence, the

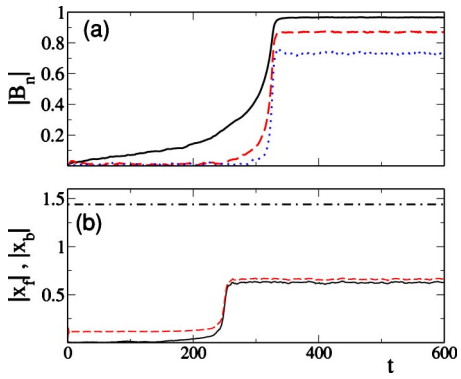

FIG. 2. Time evolution of amplitude of the first Fourier modes of the θ distribution ($n=1,2,3$ correspond to solid, dashed, and dotted curves, respectively). (b) Rise of both amplitudes (solid and dashed lines corresponds to $|x_b|$ and $|x_f|$, respectively). The dot-dashed line represents the injected field Y. The parameter values are $\Delta_a=-30$, $\Gamma_\perp=1$, $\Gamma_\parallel=2$, $\tilde{C}=7.1$, $\Delta_c=0$, $G=54$, $Y=1.45$, $\gamma_c=1/3$, and $T=5\times10^{-2}$.

mere numerical observation of a stable, steady bunching represents an important step toward generalizing the CARL predictions [8].

Such an observation is, however, not sufficient in itself. The question arises naturally whether the backward field originates from the growth of a nonhomogeneous longitudinal atomic distribution, or whether the spatial inhomogeneity results as a consequence of a preexisting optical standing wave, generated by other source terms. Although apparently obvious, this point is far from being trivial. Indeed, any standing wave is going to generate a whole hierarchy of gratings (atomic polarization and inversion, index of refraction, and—if the atoms are free to move—atomic density), but one needs to identify the true source. In this system, a source term which gives rise to a collective state has already been identified in the nontrivial grating in the atomic polarization's phase [16,18], while a standard polarization modulation (without phase transition) has been proposed [14] as a possible mechanism for interpreting the experimental observations [11,12].

In order to characterize the appearance of a spatial inhomogeneity in the atomic distribution, we introduce the characteristic function of the position (z_j) distribution defined in terms of its Fourier modes

$$B_n := \frac{1}{N}\sum_{j=1}^{N} e^{2ikz_j}. \tag{4}$$

Introducing the normalized variable θ, the general definition Eq. (4) reads, with our normalization,

$$B_n = \langle e^{2in\theta}\rangle. \tag{5}$$

The direct integration of model (1), using the same techniques as outlined in [16] (i.e., with thermalization induced by collisions), provides the results shown in Fig. 2. 2(a) shows the appearance of several Fourier modes, which reach a steady state amplitude after the backward field has grown to its final value [Fig. 2(b)(b), solid line]. We stress that the latter grows from zero spontaneously, without any *seed* injected in the computation.

From Fig. 2(a) we remark that one Fourier component of the atomic spatial distribution significantly grows away from zero well before the backward field begins to deviate from its initial value. We will take this as a suggestion, to be later verified, that the bunching is responsible for the appearance of the counterpropagating field. The harmonic components, instead, appear to be generated by the interaction of the inhomogeneously distributed atoms and the optical standing wave, generated by the two macroscopic counterpropagating fields x_f and x_b. In addition, we also see how the forward field [dashed line in Fig. 2(b)] is modified by the presence of the spatially modulated atomic distribution.

The physical picture described by this figure is the following. The cavity initially contains the atoms and no fields. At time $t=0$, we start injecting the external component Y, collinear with the forward direction. During the transient preceding synchronization, the atoms use part of the energy to adapt their positions and velocities, thus building up a nonhomogeneous spatial distribution. We remark that the total energy injected into the cavity (see dot-dashed line) is larger than that contained in the two field components at steady state ($t>300$ time units). The fact that both fields x_f and x_b grow nearly to the same value implies that one cannot neglect the dynamics of the forward field. This dynamics maximizes the spatial modulation and *both* fields adapt themselves to the global coupling that ensues. It is also crucial to remark that, although the spatial atomic inhomogeneity appears to be responsible for the generation of the backward field, at time $t\approx230$ time units, the B_1 component has reached only one-third of its final value. Hence, the rest of the modulation (fundamental plus all the harmonics) results from the interaction with the optical standing wave. This point is significant, since it implies that the scattering from one field into the other is going to be quite symmetric: any increase in one component will imply a larger number of photons in one direction and hence a larger scattered contribution from that direction into the other. The residual difference between the forward [dashed line, Fig. 2(b)] and the backward fields is to be attributed to the fact that the former receives an additional contribution from the external injection; hence the corresponding mode contains more photons at any time.

A more convincing illustration of the active role played by the density grating in the generation of the backward field can be gained by decomposing the "force" field acting on the intensity $|x_b|^2$ of the backward field into two contributions,

$$\frac{d|x_b|^2}{dt} = \mathcal{F}(x_f,x_B) = -2|x_b|^2 + \mathcal{F}_A(x_f,x_b), \tag{6}$$

where $\mathcal{F}_A(x_f,x_b)=2\tilde{C}\mathrm{Re}(\langle se^{i\theta}\rangle x_b^*)$. The first term on the right-hand side, due to cavity losses, always has a stabilizing effect, while $\mathcal{F}_A(x_f,x_b)$, which accounts for the atomic contribution, can be either stabilizing or destabilizing. In order to gain some insight into the resulting dynamics, we compare the force fields generated in the presence and in the absence of bunching, respectively. We do this under the assumption

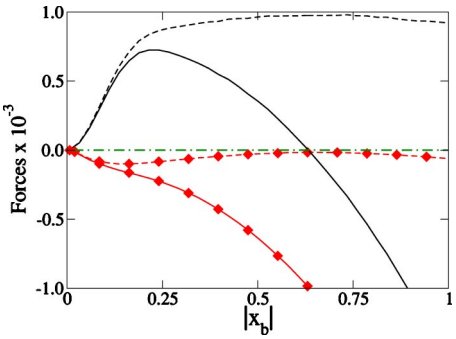

FIG. 3. The force $\mathcal{F}_A$ (dashed lines) and $\mathcal{F}$ (solid lines) versus the backward field amplitude x_b. Curves with no symbols correspond to the simulation of the full model; diamonds display curves obtained by imposing a flat distribution of positions θ (same parameter values as in Fig. 2).

that the atomic degrees of freedom can be neglected [28], i.e., that the relevant dynamical properties are contained in the dependence of $\mathcal{F}_A$ on x_b and x_f. As long as the atomic variables rapidly converge to a stationary state, one can treat $|x_f|$ and $|x_b|$ as if they were fixed parameters and thereby numerically determine the "force" field for different choices of the two amplitudes. In principle, one should also take care of the time dependence associated with the detuning ν between the two fields; however, numerical simulations of the full model have revealed that the "force" field depends very weakly on ν. The force resulting for the same parameter values as in Fig. 2 is plotted in Fig. 3 for different values of the backward field amplitude. The solid line with no symbols represents the total effective "force" acting on the backward field. Steady state operation exists only when the resulting total force is zero, and its stability is obviously determined by the local slope. It is clear that the zero-field state is unstable, while $|x_b| \approx 0.6$ is a stable one. In this latter regime, one can state that the destabilizing action of the atomic contribution $\mathcal{F}_A$ (dashed curve without symbols in Fig. 3) is balanced by the stabilizing effect due to the cavity loss term $|x_b|^2$.

In order to test the *true role* played by the atomic bunching (i.e., as a *master* or a *slave* variable), we have proceeded to "switch off" both collisions and optical forces acting on the atoms (this is obviously possible only in a simulation). The corresponding curves representing $\mathcal{F}_A$ (dashed line in Fig. 3) and the total force $\mathcal{F}$ (solid line) are identified by symbols. As a result of the absence of external perturbations, each atomic position θ_j evolves linearly according to the velocity value at the "switch off" time. In this way, the density grating is rapidly washed out. This procedure allows us to separate the possible gain component coming from the density grating from the one arising in a pumped ensemble of two-level systems [2]. The stationary value of $\mathcal{F}_A$ under such conditions always remains negative (so does a *fortiori* the total force), indicating that the presence of a density grating is an *indispensable* ingredient for maintaining a finite backward field. Notice that this is at variance with the transition studied in [16], where the force field would be positive even in the absence of a density grating [18]. Hence, we can safely conclude that the onset of a finite backward field is a clear example of a CARL and that the steady state bunching obtained is the cause of the appearance of the backward field component, and not a consequence of the existence of an optical standing wave (cf., e.g., [14]) in the parameter range that we are investigating.

IV. LARGE DETUNING LIMIT

In Sec. III we have just reported purely numerical observations. With the perspective of constructing an analytical description of the transition, it is important to identify the possibly few relevant variables. For this purpose we concentrate on the large detuning limit, where the standard adiabatic elimination holds. Although this allows us to treat analytically only a limiting case, we will draw from it the benefit of later comparing the predictions of this approach to the recent experimental observations [15], obtained with very large detuning between field and atoms ($\Delta_a \approx 10^6 \gg 1$). A discussion of the predictions resulting from such an analysis will be offered in Sec. V.

By setting, in Eqs. (1), $\dot{d}_j = \dot{s}_j = 0$, expanding the solutions in powers of $1/\Delta_a$ (to be considered as a smallness parameter), and considering first-order terms, one finds $d_j = -1$ and

$$s_j = -\frac{iG}{\Delta_a}(x_f e^{i\theta_j} + x_b e^{-i\theta_j}). \tag{7}$$

Accordingly, our model Eqs. (1) reduces to the following set of equations:

$$\dot{\theta}_j = p_j,$$

$$\dot{p}_j = \mathrm{Im}(x_f x_b^* e^{2i\theta_j}),$$

$$\dot{x}_f = -[(1 + i\bar{\Delta})x_f - Y + iCx_b B_{-1}],$$

$$\dot{x}_b = -[(1 + i\bar{\Delta})x_b + iCx_f B_1], \tag{8}$$

where $C = \tilde{C}G/\Delta_a$, and $\bar{\Delta} = \Delta_c + C$ accounts for the combined effect of atomic and cavity frequency shifts in the absence of bunching (i.e., $B_1 = B_{-1} = 0$). The above form is similar to the one discussed in [29], which was, however, obtained by phenomenologically adding relaxation terms to a single-pass model [30].

A. Vlasov model

It is now convenient to pass to a Vlasov-like description by introducing the distribution $Q(\theta, p)$ of positions and momenta. In order to simplify the analysis we now assume that the atomic positions are also randomized in each collision [31]. Accordingly, we can write

$$\partial_t Q + p\partial_\theta Q + \mathrm{Im}(x_f x_b^* e^{2i\theta})\partial_p Q = -\gamma_c(Q - Q_0), \tag{9}$$

where ∂_y denotes the partial derivative with respect to y. In the absence of a backward field, $Q(\theta, p)$ converges toward the equilibrium distribution Q_0.

We now study the stability of the solution $x_f = Y/(1 + i\bar{\Delta}) := Y_0$, $x_b = 0$, and $Q = Q_0$, by introducing the perturba-

tions δx_f, δx_b, and δQ. Since the equation for x_f depends on the other variables only at second order in the perturbations, it can be solved separately. Moreover, δx_f affects δx_b only at second order, so that it can be factored out. Therefore, the stability of δx_f justifies the assumptions made in deriving the single-pass model where x_f is considered to be a constant parameter [8,16,18]. One is thus left with the following two equations:

$$\dot{\delta x}_b = -(1+i\overline{\Delta})\delta x_b - iC\overline{Y}\delta B_1, \tag{10}$$

$$\partial_t \delta Q = -\partial_p Q_0 \mathrm{Im}(\overline{Y}\delta x_b^* e^{2i\theta}) - (\gamma_c + p\partial_\theta)\delta Q. \tag{11}$$

From the structure of these equations we see that if the bunching is washed out, i.e., $B_{\pm 1}=0$ and $\delta Q=0$, no instability can be expected in this regime. This is at variance with the case discussed in [16,18] where the effective stability of x_b can be turned into an instability sufficiently close to the atomic resonance.

From Eq. (10), one realizes that the coupling occurs through the first Fourier mode of the density distribution. One can thus solve the above equation by introducing the following *Ansätze*:

$$\delta Q(\theta,p,t) = \mathcal{Q}(p)e^{-2i\theta+\lambda t} + \text{c.c}, \quad \delta x_b = E_b e^{\lambda t}, \tag{12}$$

where λ is a complex stability eigenvalue. After substituting the above expressions into Eqs. (10) and (11) and equating terms with the same exponential factor, one finds

$$(\lambda + 1 + i\overline{\Delta})\mathcal{E}_b + 2i\pi C\overline{Y}\int_{-\infty}^{\infty} dp\,\mathcal{Q}(p) = 0, \tag{13}$$

$$\frac{i}{2}\overline{Y}^*\mathcal{E}_b\partial_p Q_0 + (\lambda - 2ip + \gamma_c)\mathcal{Q} = 0. \tag{14}$$

By solving Eq. (14) and replacing into Eq. (13), one obtains the solvability condition

$$\lambda = -(1+i\overline{\Delta}) - \pi C|\overline{Y}|^2 \int_{-\infty}^{\infty} dp \frac{\partial_p Q_0}{\lambda - 2ip + \gamma_c}. \tag{15}$$

Within this framework, the onset of both bunching and backward field is signaled by a change of sign of the real part of λ, λ_r [32]. The integral in Eq. (15) can be analytically expressed using an error function. Nevertheless, this would hide an important point. Let us place ourselves at threshold and rewrite Eq. (15), assuming that λ is purely imaginary. Setting $\lambda=-i\beta$, we obtain for the real part

$$0 = -1 + \pi\frac{C\gamma_c|\overline{Y}|^2}{T\sqrt{2\pi T}}\int_{-\infty}^{\infty} dp \frac{pe^{-p^2/(2T)}}{(\beta+2p)^2+\gamma_c^2}. \tag{16}$$

In order for such an equation to be valid, the condition

$$\int_{-\infty}^{\infty} dp \frac{pe^{-p^2/(2T)}}{(\beta+2p)^2+\gamma_c^2} > 0 \tag{17}$$

must be satisfied. The numerator is an odd function of p. The sign of the integral in Eq. (17) is thus determined by the denominator, whose minimum is reached at $p_0=-\beta/2$. Finally, Eq. (17) imposes $\beta<0$. From the sign convention adopted here (the same as in Ref. [17]), a complex field E, of frequency ω, is linked to its slowly varying envelope A through $E=A\exp[-i\omega t]$. Thus β physically represents the detuning between the backward field and the forward field. One can therefore conclude that the spontaneous symmetry breaking, causing x_b to grow, can give rise to only a red-detuned field.

B. Fokker-Planck description

We now turn to analyzing the relaxation mechanism that most closely models the recent experimental results [15]. There, the cw superposition of additional laser beams, tuned to the D_2 transition of rubidium, introduces a mechanism that slows down those atoms which would be accelerated away from resonance by the strong interaction arising from CARL. Indeed, it was reported [15] that in the absence of the molasses only transient backward emission could take place (and its interpretation as CARL is complicated by the technique used for preparing the sample, which pre-traps the atoms in a standing wave). The key point in the experiment is that the molasses is always present during the interaction but on the other D line (the experiment being done on D_1).

In the large detuning limit, the second of Eqs. (8) is replaced by

$$\dot{p}_j = \mathrm{Im}(x_f x_b^* e^{2i\theta_j}) - \gamma p_j + \eta_j(t). \tag{18}$$

Equation (18) describes the evolution of (θ, p) in a potential self-consistently determined by the dynamics of the two counterpropagating field components x_f and x_b, which in turn depends on the joint distribution $Q(\theta,p)$. The evolution of Q corresponding to Eq. (18) is given by the Fokker-Planck equation

$$\partial_t Q + p\partial_\theta Q + \mathrm{Im}(x_f x_b^* e^{2i\theta})\partial_p Q = \gamma\partial_p(pQ + T\partial_p Q). \tag{19}$$

Notice that this equation differs from the Vlasov equation (9) only for the relaxation terms contained in the right-hand side.

By proceeding as in the previous subsection, we linearize Eq. (19), obtaining

$$\partial_t \delta Q = -\partial_p Q_0 \mathrm{Im}(\overline{Y}\delta x_b^* e^{2i\theta}) - p\partial_\theta\delta Q + \gamma\partial_p(p\delta Q + T\partial_p\delta Q), \tag{20}$$

which is to be compared to the corresponding Eq. (11) in the Vlasov description [the linearised x_b equation, being identical to Eq. (10), is not repeated]. Using the *Ansätze* (12), we finally find

$$\frac{i}{2}\overline{Y}^*\mathcal{E}_b\partial_p Q_0 + (\lambda - 2ip - \gamma)\mathcal{Q} - \gamma(p\partial_p\mathcal{Q} + T\partial_p^2\mathcal{Q}) = 0, \tag{21}$$

which is to be solved together with the first of Eqs. (21). In view of its differential structure, it is doubtful whether a general analytic solution can be found, and the development of a numerical analysis would be a quite delicate task as well. Nevertheless, in the "strong friction" (SF) limit, the atomic momentum can be adiabatically eliminated, and one

can thereby perform a quite detailed investigation of the transition scenario. While a careful discussion of the adiabatic elimination in the presence of noise can be found in Ref. [33], here we limit ourselves to presenting a sketchy but substantially correct derivation where we set $\dot{p}=0$ in Eq. (18). By proceeding in this way, one obtains the Langevin equation

$$\dot{\theta}_j = \frac{1}{\gamma}\mathrm{Im}(x_f x_b^* e^{2i\theta_j}) + \frac{\eta_j}{\gamma}, \tag{22}$$

equivalent to the one-variable Fokker-Planck (Smoluchowski) equation [33]

$$\partial_t \rho + \frac{1}{\gamma}\partial_\theta \mathrm{Im}(x_f x_b^* e^{2i\theta})\rho - \frac{T}{\gamma}\partial_\theta^2 \rho = 0 \tag{23}$$

for the variable ρ,

$$\rho(\theta) = \int_{-\infty}^{\infty} Q(\theta,p)dp. \tag{24}$$

We remark that Eq. (22), which describes the dynamics of an ensemble of mean field coupled oscillators, belongs to the class of Kuramoto systems [34]. The main differences are a Dirac-like distribution of eigenfrequencies and a mean field self-consistently provided by a dynamical equation. By paralleling the approach in Sec. IV A, the stability of the solution $x_f=\overline{Y}$, $x_b=0$, $\rho=1/2\pi$ can be studied by introducing the infinitesimal perturbations δx_b and $\delta\rho$. The linearization of Eq. (23) yields

$$\partial_t \delta\rho = -\frac{1}{2\pi\gamma}\partial_\theta \mathrm{Im}(\overline{Y}\delta x_b^* e^{2i\theta}) + \frac{T}{\gamma}\partial_\theta^2 \delta\rho. \tag{25}$$

Upon the insertion of the *Ansätze* $\delta\rho = re^{-2i\theta+\lambda t} + \mathrm{c.c.}$ and $\delta x_b = \mathcal{E}_b e^{\lambda t}$ into the above equation, one obtains

$$r = -\frac{\mathcal{E}_b \overline{Y}^*}{2\pi}\frac{1}{\lambda\gamma + 4T}, \tag{26}$$

and from the linearized equation for the field dynamics, Eq. (10),

$$\lambda = -(1 + i\overline{\Delta}) + i\frac{C|\overline{Y}|^2}{\lambda\gamma + 4T}, \tag{27}$$

where now

$$B_{\pm 1} = \int_0^{2\pi} e^{\pm 2i\theta}\rho(\theta)d\theta. \tag{28}$$

The threshold can now be obtained by setting $\lambda=-i\beta$ (where β is a real number) in Eqs. (26) and (27). The resulting two real equations for β and $|\overline{Y}|$ are

$$\gamma\beta^2 - \overline{\Delta}\gamma\beta - 4T = 0, \tag{29}$$

$$-\beta(\gamma + 4T) + 4\overline{\Delta}T = C|\overline{Y}|^2. \tag{30}$$

Only the negative β solution of Eq. (29) leads to a physically acceptable solution $|\overline{Y}|^2 > 0$. The threshold equations finally read

$$\beta_{TH} = \frac{\overline{\Delta}}{2} - \sqrt{\left(\frac{\overline{\Delta}}{2}\right)^2 + 4\frac{T}{\gamma}},$$

$$|\overline{Y}_{TH}|^2 = \frac{\overline{\Delta}}{2C}(4T-\gamma) + \frac{1}{C}(4T+\gamma)\sqrt{\left(\frac{\overline{\Delta}}{2}\right)^2 + 4\frac{T}{\gamma}}. \tag{31}$$

The first equation shows that the probe field is *always* red detuned at threshold. This result is in agreement with the outcome of the Vlasov model (see Sec. IV A) even though these two models correspond to different thermalization mechanisms. In the case of a resonant cavity field $\overline{\Delta}=0$, the above equations reduce to

$$\beta_{TH} = -2\sqrt{\frac{T}{\gamma}}, \tag{32}$$

$$|\overline{Y}_{TH}|^2 = \frac{2}{C}(4T+\gamma)\sqrt{\frac{T}{\gamma}}. \tag{33}$$

In the SF limit, one can not only determine analytically the threshold condition, but also go beyond, describing the regime above threshold. By inserting the expansion of ρ,

$$\rho(\theta,t) = \sum_{n=-\infty}^{\infty} f_n(t)e^{in(2\theta+\beta t)}, \tag{34}$$

into Eq. (23), one obtains the recurrence relation

$$\gamma\dot{f}_n = -in\gamma\beta f_n - n[Rf_{n-1} - R^* f_{n+1}] - 4Tn^2 f_n, \tag{35}$$

where we have set $x_f x_b^* = Re^{i\beta t}$, R being a complex constant. For $n>0$, the stationary state is given by

$$(4Tn + in\gamma\beta)f_n + [Rf_{n-1} - R^* f_{n+1}] = 0. \tag{36}$$

By introducing $Z_n = R^*(f_{n+1}/f_n)$ and solving the equation by means of the continuous fraction method, we obtain the recurrence relation

$$Z_{n-1} = \frac{|R|^2}{Z_n - (4Tn + in\gamma\beta)}. \tag{37}$$

The normalization condition for ρ gives $2\pi f_0 = 1$, while the atomic contribution for x_b and x_f can then be determined from Eq. (28),

$$B_1 = 2\pi f_{-1}e^{-i\beta t} = \frac{Z_0^*}{R}e^{-i\beta t},$$

$$B_{-1} = 2\pi f_1 e^{i\beta t} = \frac{Z_0}{R^*}e^{i\beta t}. \tag{38}$$

This method enables us to go beyond the linear analysis, determining the dependence of both x_f and x_b on the injected

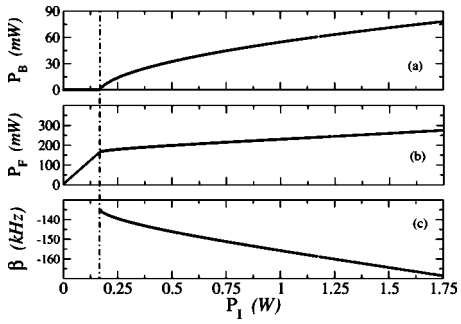

FIG. 4. Bifurcation diagram numerically computed using the Fokker-Planck model. (a), (b), and (c) present the backward field power P_B, the forward field power P_F, and the detuning between backward and forward field, β, as functions of the injected power P_I, respectively. All quantities are in physical units. The parameter values used for the simulations correspond to those of the experiment [15].

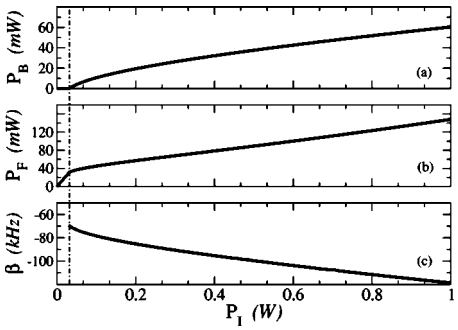

FIG. 5. Bifurcation diagram numerically computed using the Vlasov model. (a), (b), and (c), present, respectively, the backward field power P_B, the forward field power P_F, and the detuning between backward and forward field, β, as functions of the injected power P_I. All quantities are in physical units. The parameter values used for the simulations correspond to those of the experiment [15].

field (see Sec. V), with the only restriction that Z_0 has to be computed numerically.

V. PREDICTIONS

In this section we discuss the results derived in Sec. IV in the large detuning limit for both the Fokker-Planck (see Sec. IV B) and Vlasov (Sec. IV A) models. We first test the validity of the two approaches by comparing them to the experimental results of Ref. [15]. The experiment was performed with cold ^{85}Rb atoms in a high-Q ring cavity. The atomic parameters are $m=1.4\times10^{-25}$ kg, $\mathcal{D}=1.5\times10^{-29}$ C m^{-1} with relaxation rates for atomic polarization and inversion $2\gamma_\perp=\gamma_\parallel=5.9$ MHz, respectively. Moreover, the atomic frequency is $\omega=3.77\times10^{14}$ Hz (for the D_1 line), while the input field is shifted 1 THz away from it. The beam diameter is 130 μm. The cavity linewidth is 22 kHz, the transmissivity $\mathcal{T}=1.8\times10^{-6}$, and the medium's length $L=10^{-3}$ m. Since a servo-mechanism continuously adapts the dressed cavity resonance to the frequency of the injected field, we assume $\bar{\Delta}=0$.

The equilibrium gas temperature, in the absence of collective interaction, is experimentally known with a large uncertainty. We use an estimated value $\bar{T}\approx250$ μK, which lies within the range of uncertainty. The second crucial parameter that characterizes the thermalization is the damping constant, experimentally evaluated in Ref. [15] to be $\gamma=9$. We will thus use $\gamma=\gamma_c=9$.

We first report the results of the Fokker-Planck model since it describes more appropriately the molasses dynamics. In Fig. 4(a) one remarks, from the shape of the backward field power, the existence of a continuous phase transition. The threshold is located at $P_I\approx0.2$ W, compatible with the measurements of Ref. [15], which reports backward lasing as occurring for a few watts of injected power.

The possible underestimate in the threshold value that we obtain from our approach can be attributed to two experimental features that cannot be taken into account in a simple way. First, the servo control, which keeps the cavity on resonance by *maximizing the forward transmitted field* [15], cannot be correctly modeled by simply setting $\bar{\Delta}=0$. Indeed, its operation amounts to a dynamical process which counteracts the creation of the backward emission, since the latter removes energy from the forward field. As a result, one expects the threshold to be displaced toward higher input power values. Second, the spatial modulation imprinted onto the sample by the molasses beam, with a wavelength that differs from that of the collective process (by a factor close to $\sqrt{2}$), introduces a competition between two incompatible length scales. It is likely that this effect may contribute to raising the critical input power even further.

The detuning value β at which the backward field arises [cf. Fig. 4(c)] agrees with the observations [15], which report a redshift around 100 kHz. Finally, the continued fraction expansion discussed in the previous section allows for a determination of the behavior of the forward field as a function of the input power [cf. Fig. 4(b)]. Below threshold, P_F grows linearly as a function of the injected power P_I, as no energy is transferred to the backward field. Above threshold, a fraction of the injected field feeds the backward mode, thus leading to a slower growth of P_F.

Although one does not expect the Vlasov description to closely reproduce the experimental results reported in Ref. [15], it is worth analyzing its predictions; this will help us in clarifying the role of the relaxation mechanisms and will sharpen our understanding of the problem. From Fig. 5 one sees that, for the same parameter values used in the Fokker-Planck approach, the threshold is somewhat lower and the redshift in the backward field frequency is smaller as well. Nevertheless, the differences are not very dramatic, since, while the threshold occurs for somewhat lower values of the input power, the frequency shift shows an even somewhat better agreement with the observations [15]. In addition, the uncertainty in some of the experimental parameters is large enough to render a sure discrimination between the modeling based on a Vlasov or on a Fokker-Planck process quite difficult. Because of the intrinsic paradox, given by the inclusion in the experiment of the optical molasses which ought to exclude the Vlasov description, this result strongly indicates that the current state of the system's characterization, both

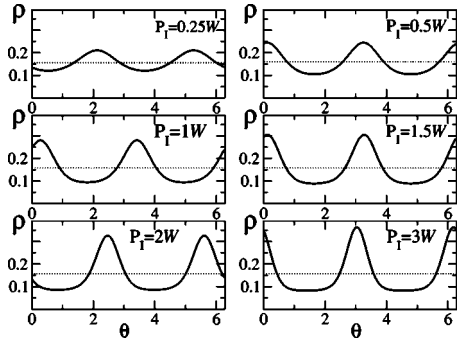

FIG. 6. Position distribution $\rho(\theta)$, for different values of the injected power P_I, in physical units. In each part of the figure, the dotted line corresponds to the uniform distribution. The parameter values used for the simulations correspond to those of the experiment [15].

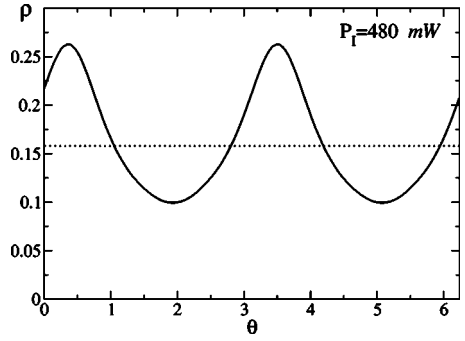

FIG. 8. Atomic position distribution $\rho(\theta)$, as function of θ, above threshold. The dotted line corresponds to the uniform distribution, below threshold.

experimental and theoretical, is not adequate; hence, a large amount of caution in drawing conclusions ought to be exercised.

In addition to the direct comparison to the experiment, we can also examine some specific predictions coming from each model. The distribution of atomic positions ρ predicted by the Fokker-Planck model is plotted in Fig. 6: the different parts of the figure correspond to increasing values of the injected power P_I (the other parameters remaining unchanged). One can clearly see the rise of the modulation with an increasing role played by higher harmonics.

In the Vlasov description, there is no equivalent regime characterized exclusively by the distribution of θ values. The probability density $Q(\theta,p)$ for an input intensity above threshold is plotted in Fig. 7, where one can indeed appreciate the need to account for both the p and θ dependence in this framework. Nevertheless, one can compute $\rho(\theta)$ by integrating $Q(\theta,p)$ [see Eq. (24)]. The results, plotted in Fig. 8, reveal again a qualitative agreement with the Fokker-Planck approach. The larger modulation for the same input power is a consequence of the smaller value of the threshold in the Vlasov description.

VI. CONCLUSIONS AND PERSPECTIVES

In this paper we have presented a general framework for the description of the spontaneous appearance of a stationary density grating arising from the interaction between an atomic sample enclosed in a bidirectional ring cavity and an injected, quasiresonant field. This contribution completes the picture previously sketched out in Refs. [16,18], where we showed that the inclusion of a relaxation mechanism for the external degrees of freedom is indispensable for a correct modeling of the interaction, and is responsible for the appearence of a stationary backward field. In the previous work, we focused on the existence of a different kind of phase transition, initiated by a grating in the phase of the atomic polarization. Here, with the help of a detailed numerical analysis, we have proven beyond doubt that a true stationary CARL action—i.e., one initiated by the birth of an atomic density modulation—can spontaneously occur. For the investigation, we have chosen to study a bidirectional ring cavity model [19,17] because of the fuller and more correct description that the latter provides of a real system. In the course of the presentation, we have shown that in certain limits the ring cavity model reduces to the single-pass one [8,16,18]; this legitimizes, *a posteriori*, the use of the latter approach under such conditions.

Following a discussion of the main relaxation mechanisms that one may expect to find in an experiment, we have offered an analytical description of the two most likely ones on the basis of a probabilistic description, in the large detuning limit. Comparison between our predictions and recent experimental results [15] shows a semiquantitative agreement, surprisingly, for both the Fokker-Planck and the Vla-

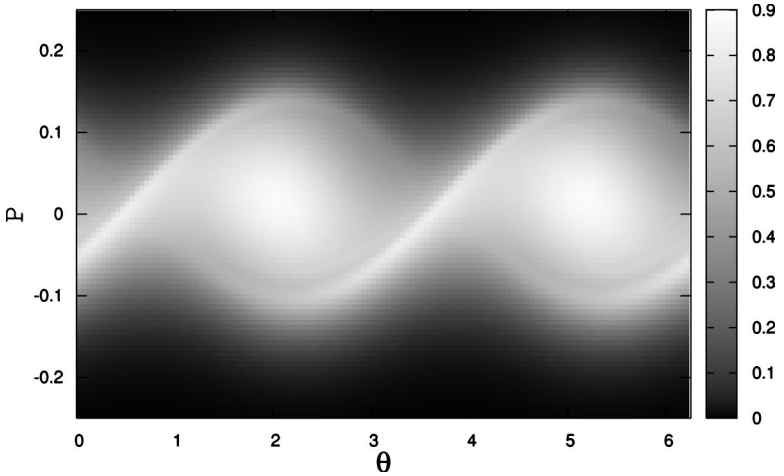

FIG. 7. Joint distribution $Q(\theta,p)$ above threshold. The parameter values are the same as those of the experiment [15] with input power equal to 480 mW.

sov approaches. In addition to the need for a more accurate experimental characterization of the phenomenon, including a better determination of the parameter values, and systematic measurements of the threshold behavior and of the functional dependence of the backward field power and frequency, additional theoretical work needs to be completed. In particular, a more accurate modeling of the relaxation mechanism represented by the optical molasses needs to be achieved, together with an analysis of the limits of validity of the descriptions proposed for the losses. Finally, it will be useful to investigate the transition scenario where the two mechanisms separately described here and in Refs. [17,19] cooperate to induce a backward field; this is likely to occur in the range of smaller detunings when the atomic variables cannot be eliminated.

ACKNOWLEDGMENTS

The authors warmly thank Ph. W. Courteille for sharing information on the experiment before publication. M.P. wishes to acknowledge the INOA for financial support and L. M. Narducci and M. Le Bellac for useful discussions. This work has been partially funded by the FIRB, Contract No. RBNE01CW3M_001.

[1] C. N. Cohen-Tannoudji, Rev. Mod. Phys. **70**, 707 (1998).
[2] S. Haroche and F. Hartmann, Phys. Rev. A **6**, 1280 (1972).
[3] D. Grandclément, G. Grynberg, and M. Pinard, Phys. Rev. Lett. **59**, 40 (1987).
[4] G. Khitrova, J. F. Valley, and H. M. Gibbs, Phys. Rev. Lett. **60**, 1126 (1988).
[5] M. T. Gruneisen, K. R. MacDonald, A. L. Gaeta, R. W. Boyd, and D. J. Harter, Phys. Rev. A **40**, 3464 (1989).
[6] J. Guo, P. R. Berman, B. Dubetsky, and G. Grynberg, Phys. Rev. A **46**, 1426 (1992).
[7] J.-Y. Courtois, G. Grynberg, B. Lounis, and P. Verkerk, Phys. Rev. Lett. **72**, 3017 (1992).
[8] R. Bonifacio and L. De Salvo, Nucl. Instrum. Methods Phys. Res. A **341**, 360 (1994); R. Bonifacio, L. De Salvo, L. M. Narducci, and E. J. D'Angelo, Phys. Rev. A **50**, 1716 (1994).
[9] P. R. Berman, Phys. Rev. A **59**, 585 (1999).
[10] L. A. Orozco, H. J. Kimble, A. T. Rosenberger, L. A. Lugiato, M. L. Asquini, M. Brambilla, and L. M. Narducci, Phys. Rev. A **39**, 1235 (1989). See Sec. V E.
[11] G. L. Lippi, G. P. Barozzi, S. Barbay, and J. R. Tredicce, Phys. Rev. Lett. **76**, 2452 (1996).
[12] P. R. Hemmer, N. P. Bigelow, and D. P. Katz, and M. S. Shahriar, L. De Salvo, and R. Bonifacio, Phys. Rev. Lett. **77**, 1468 (1996).
[13] S. Barbay, G. Fabre, and G. L. Lippi, Opt. Commun. **165**, 119 (1999).
[14] W. J. Brown, J. R. Gardner, D. J. Gauthier, and R. Vilaseca, Phys. Rev. A **55**, R1601 (1997).
[15] D. Kruse, C. von Cube, and C. Zimmermann, and Ph. W. Courteille, Phys. Rev. Lett. **91**, 183601 (2003).
[16] M. Perrin, G. L. Lippi, and A. Politi, Phys. Rev. Lett. **86**, 4520 (2001).
[17] M. Perrin, Z. Ye, and L. M. Narducci, Phys. Rev. A **66**, 043809 (2002).
[18] J. Javaloyes, G. L. Lippi, and A. Politi, Phys. Rev. A **68**, 033405 (2003).
[19] Z. Ye and L. M. Narducci, Phys. Rev. A **63**, 043815 (2001).
[20] For instance, the original model [8] , derived under the approximation of a constant input field, does not conserve energy even in the absence of dissipation
[21] J. Evans and G. P. Morriss, *Statistical Mechanics of Nonequilibrium Liquids* (Academic Press, San Diego, 1990)
[22] F. Mitschke, R. Deserno, W. Lange, and J. Mlynek, Phys. Rev. A **33**, 3219 (1986).
[23] T. Ackemann and W. Lange, Appl. Phys. B: Lasers Opt. **72**, 21 (2001).
[24] R. A. MacDonald and D. H. Tsai, Phys. Rep. **6**, 1 (1978).
[25] M. Perrin, Ph.D. thesis, Université de Nice–Sophia Antipolis, 2003 (in French).
[26] J. Javaloyes, Ph.D. thesis, Université de Nice–Sophia Antipolis, 2003 (in French).
[27] C. Cohen-Tannoudji, J. Dupont-Roc, and G. Grynberg, *Atom-Photon Interactions: Basic Processes and Applications* (Wiley, New York, 1992).
[28] While the atomic polarization and population can be safely eliminated by following the procedure described in Ref. [18] , more questionable is the treatment of position and momentum. However, preliminary investigations indicate that this is possible at least in some parameter ranges.
[29] R. Bonifacio and P. Verkerk, Opt. Commun. **124**, 469 (1996).
[30] R. Bonifacio and L. De Salvo, Opt. Commun. **115**, 505 (1995).
[31] The net effect of this randomization is to increase the threshold value of the injected field, because of the disorder introduced.
[32] An analogous stability analysis was carried out also in Ref. [29] , where, however, the possible occurrence of a phase transition was missed because of the additional presence of a probe field. In fact, as is the case in ferromagnetic systems the presence of an external field destroys the second-order transition.
[33] H. Risken, *The Fokker-Planck Equation* (Springer,Berlin, 1984).
[34] S. H. Strogatz, Physica D **143**, 1 (2000).
[35] P. R. Berman, T. W. Mossberg, and S. R. Hartmann, Phys. Rev. A **25**, 2550 (1982).
[36] P. L. Bhatnagar, E. P. Gross, and M. Krook, Phys. Rev. **94**, 511 (1954).
[37] M. Krook, Phys. Rev. **99**, 1896 (1955).